ELSEVIER

Journal of Molecular Catalysis A: Chemical 120 (1997) 33–45

JOURNAL OF MOLECULAR CATALYSIS A: CHEMICAL

EXAFS/FT-IR characterization of tetra-iridium carbonyl clusters bound to tris-(hydroxymethyl)phosphine grafted silica surface catalytically active for propene oxidation to acetone

Takafumi Shido, Takumi Okazaki, Masaru Ichikawa *

Catalysis Research Center, Hokkaido University, Sapporo 060, Japan

Received 15 September 1995; accepted 17 September 1996

Abstract

Structure and catalytic activity of $Ir_4(CO)_{12}$ bound to tris-(hydroxymethyl)phosphine (THP) grafted silica (THP/SiO_2) was investigated by means of EXAFS, FT-IR and kinetic studies. It was found that $Ir_4(CO)_{12}$ was uniformly attached on THP/SiO_2 by substitution of CO by THP ($Ir_4/THP/SiO_2$). The tetra-iridium carbonyl cluster framework was remained during the substitution of THP ligands and two THP ligands coordinated to the iridium carbonyl clusters to form $Ir_4(CO)_{10}(THP/SiO_2)_2$ species. When $Ir_4/THP/SiO_2$ was evacuated at 373 K, bridge CO was desorbed and Debye–Waller factor of Ir–Ir contribution derived from EXAFS analysis was increased which suggested that the cluster framework was distorted by the evacuation at 373 K. The resulting sample evacuated at 373 K was an active catalyst for hydroformylation of ethene and partial oxidation of propene, while the $Ir_4/THP/SiO_2$ without evacuation exhibited poor catalytic activities. The propene oxidation reaction proceed on the $Ir_4/THP/SiO_2$ evacuated at 323–353 K under subatmospheric pressures to give acetone as a product in high selectivity. The ethene hydroformylation proceed on the evacuated $Ir_4/THP/SiO_2$ at lower temperatures compared with other conventional iridium catalysts. EXAFS characterization and kinetic studies suggested that the catalytic activities were associated with the structural distortion of the iridium cluster framework due to surface attachment by the bidentate phosphine substitution.

Keywords: $Ir_4(CO)_{12}$; EXAFS; FTIR; Attached clusters on phosphine modified SiO_2

1. Introduction

Attachment of metal complexes and clusters is a useful method to construct a well defined active site of heterogeneous catalyst in molecular level [1–5]. In the early stage of the surface attached metal compounds, most of studies were stressed on the simple attachment of the metal complexes which were inherently active in homogeneous system on the oxide or organic polymer surface [6]. In the second stage of the attached metal cluster compounds, the surface grafted cluster complexes were synthesized by the reaction with surface hydroxyl groups on oxide surfaces such as SiO_2, Al_2O_3 and MgO [4,5]. It has been reported that $Ru_3(CO)_{12}$, $Os_3(CO)_{12}$, $Fe_3(CO)_{12}$ react with surface hydroxyl groups to form surface anchored hydroxylated clusters [4,5]. Further, allyl and hydrido

* Corresponding author. Tel.: +81-11-7062912; fax: +81-11-7064957.

PII S1381-1169(96)00412-8

complexes such as $Mo_2(\eta^3\text{-}C_3H_5)_4$ and $Cr(\eta^3\text{-}C_3H_5)_3$ were attached on the oxide surfaces using the dehydrogenation with surface hydroxyl groups [3,6]. The attempt of the synthesis of surface bound metal complexes and metal cluster emerged a new area of chemistry called 'surface organometallic chemistry'.

For iridium carbonyl clusters, structural transformation of supported $Ir_4(CO)_{12}$ on SiO_2 [7], Al_2O_3 [8], and MgO [9–12] have been widely investigated. $Ir_4(CO)_{12}$ was generated on Al_2O_3 surface by the reductive carbonylation of $[Ir(CO)_2(acac)]$. $Ir_4(CO)_{12}$ impregnated on Al_2O_3 was converted to Ir_4 metal aggregates by decarbonylation at 573 K under helium. $Ir_4(CO)_{12}$ on MgO reacts with surface OH groups to form $[HIr_4(CO)_{11}]^-$. Gates et al. reported that iridium carbonyl clusters such as $Ir_4(CO)_{12}$ and $Ir_6(CO)_{16}$ were synthesized from $[Ir(CO)_2(acac)]$ and $[HIr_4(CO)_{11}]^-$ in NaY zeolite cages [13,14] and that $[Ir_6(CO)_{15}]^{2-}$ were synthesized in NaX zeolite [15], which have been characterized by EXAFS and IR.

Since the surface reactions of metal complexes and metal cluster compounds depend on the nature of the oxide surfaces, the subtle control of the structure of attached metal compounds is difficult. To make a crucial structure control of the surface attached metal cluster compounds, one possible method is proposed as follows; (1) Grafting of ligands with short carbon chain on oxide surfaces whose amount is controlled so that inter ligands distance would be slightly longer than that in solution. (2) When the metal complexes and cluster is coordinated by two or three surface fixed ligands, the metal compound should be tensed, resulting in the structural distortion of the metal cluster framework. It is of interest to investigate the structure of surface bound metal clusters modified by the functionalization of the oxide surface which may be reflected in the catalytic performances.

In the previous study we have reported the functionalization of silica surface using tris-(hydroxymethyl)phosphine ($P(CH_2OH)_3$, THP) and attachment of $Rh_4(CO)_{12}$ on the functionalized silica surface (THP/SiO_2) [16–18]. Attached tetra-rhodium carbonyl clusters were coordinated by two THP ligands and the cluster framework was distorted by the tension from surface fixed THP ligands. The attached rhodium clusters on THP/SiO_2 were as active as Wilkinson complex $(HRh(CO)Cl(PPh_3)_2$, one of the most active catalyst for hydroformylation) in hydroformylation reaction and the selectivity for aldehyde formation was more than 98%. Comparison of the activity with undistorted tetra-rhodium clusters such as $Rh_4(CO)_{10}(THP)_2$ in solution revealed that the surface bound clusters with a distortion of the cluster framework exhibited remarkable catalytic activities for the selective hydroformylation reaction of olefins [16–18].

Along with this, it is interesting to extend to other metals such as iridium carbonyl clusters to study the generation of catalytic active sites due to the distortion of cluster framework. It may be relevant to the rational design of active site for heterogeneous catalyst.

Accordingly, in this paper we have tried to synthesize the surface-bound $Ir_4(CO)_{12}$ on the THP grafted silica which have been characterized using EXAFS and FTIR. The structures of surface-bound tetra-iridium carbonyl clusters were discussed in the conjunction with the catalytic activities in the ethene hydroformylation reaction and propene oxidation reaction.

2. Experimental

Functionalization of silica surface was performed by the thermal treatment of THP with silica gel in the same method reported previously [16–18]. Briefly, THP is obtained by reflex of tetrakis-(hydroxy-methyl)phosphonium chloride (supplied by Albright and Wilson) with NEt_4OH [19]. Grafting of THP on silica was performed as follows; an ethanol solution of THP was mixed under nitrogen with SiO_2 (Aerosil 200, evacuated at 473 K). Then the

ethanol was evaporated at room temperature followed by evacuation at 403 K (THP/SiO_2). The loading of THP was 6.2 wt%, which was the maximum amount of THP loaded on silica surface.

$Ir_4(CO)_{12}$ and THP/SiO_2 was mixed and refluxed in hexane for 24 h under nitrogen. The sample color was changed from pale yellow to orange which was the characteristic color of phosphine substituted tetra-iridium carbonyl clusters. Different from the case of $Rh_4(CO)_{12}$, $Ir_4(CO)_{12}$ did not react with THP/SiO_2 at room temperature because of low solubility of this compound. Heating of the mixture of $Ir_4(CO)_{12}$ and THP/SiO_2 at the boiling point of hexane is an analogy of the method of the synthesis of $Ir_4(CO)_8(PPh_3)_4$ in which mixture of $Ir_4(CO)_{12}$ and triphenylphosphine was heated at the boiling point of toluene [20]. Loading of iridium metal was 3.0 wt%. Kinetic studies were carried out using a closed circulating reactor made by Pyrex glass whose dead volume being 206 cm^3. About 0.2 g of the catalyst was charged in a Pyrex U-shape tube. Ethene hydroformylation reaction and propene oxidation reaction were carried out at 323–353 K, $p(H_2) = p(CO) = p(C_2H_4) = 13.3$ kPa and at 323–353 K, $p(C_3H_6) = p(O_2) = 13.3$ kPa, respectively. Products were analyzed using gas chromatography (Shimadzu GC-8A). Column FFAP (4 m) was used to separate oxigenated compound such as acetone, propanal, and propanol, and Unibeads 1S (2 m) was used to separate hydrocarbons and inorganic gases, such as CO, CO_2, H_2, O_2, C_2H_4, C_2H_6, and C_3H_6. Column temperature was set at 353 K. Turn over frequencies (TOF) were calculated by the division of reaction rate into total iridium atoms.

IR spectra was measured at 300 K or reaction temperatures using Shimadzu FTIR-4100 with resolution of 2 cm^{-1}. About 30 mg of the sample was pressed into a self-supporting disk and mounted in a Pyrex made IR cell which was connected to a vacuum system. Background of silica support and gas phase absorption were subtracted in each spectrum.

Ir L_{III} edge EXAFS (extended X-ray absorption fine structure) spectra were measured at BL-10B at Photon Factory, National Institute for High Energy Physics. Positron energy and current in the ring were 2.5 GeV and 340–240 mA, respectively. X-ray adsorption spectra were measured with transmittance mode. A Si(311) channel cut monochromator was used. X-ray intensity of I_0 (before the sample) and I_t (after the sample) were measured by ionization chambers charged in 300 V filled with mixed gases of Ar and N_2. The path length of the ion chambers were 17 and 31 cm for I_0 and I_t, respectively. The concentration of Ar of the mixed gases for I_0 and I_t were 15 and 50%, respectively. The sample was mounted in an in-situ cell with Kapton (rtm) windows. The samples were sealed under vacuum and the EXAFS spectra were measured without exposure the samples to air. The thickness of the cell was 10 mm.

The analysis of X-ray absorption spectra was carried out using the program provided from Technos. EXAFS function was extracted by the subtraction of background using Victreen function and cubic sprain method. k^3 weighted EXAFS function ($\chi(k) \times k^3$) was Fourier transformed and the Fourier transformed function was filtered and inverse Fourier transformed to k-space. The k-range of Fourier transform and R range of inverse Fourier transform were 3.5–15 $Å^{-1}$ and 1.2–3.2 Å respectively. The filtered EXAFS functions were fitted by the sum of calculated EXAFS functions of Ir–Ir, Ir–P, Ir–C, and Ir–O. The calculated EXAFS functions were derived using single scattering plane wave theory [21,22]. The fitting parameter were coordination number (CN), average absorber-backscatterer distance (R), correction of inner potential (ΔE_0), and relative Debye–Waller like factors ($\Delta\sigma$) to that of reference compounds.

Backscattering amplitudes and phase shift functions were derived from reference compounds, those of Ir–Ir, Ir–P and Ir–CO were obtained from EXAFS spectra of Ir foil, $[H_2Ir(CO)(PPh_3)_3]SiF_5$, and $W(CO)_6$, respec-

Table 1
Crystallographic data characterizing the reference compounds and Fourier transform ranges used in the EXAFS analysis [a]

Sample	Crystallographic data			Fourier transform		
	Shell	CN	R/Å	Δk/Å^{-1}	ΔR/Å	n
Ir powder	Ir–Ir [e]	12	2.7147	3.5–18.0	1.9–3.0	3
$[H_2Ir(CO)(PPh_3)_3]SiF_5$ [c]	Ir-P [f]	3	2.37	3.5–18.0	1.6–2.4	3
$W(CO)_6$ [d]	W–C [g]	6	2.063	3.5–18.0	1.2–2.1	3
	W–O [h]	6	3.206	3.5–18.0	2.1–3.3	3

[a] Notation:CN, coordination number for absorber–backscatterer pair; R, absorber–backscatterer distance; Δk, limits used for forward Fourier transformation; ΔR limits used for shell isolation (R is distance); n, power of k used for Fourier transformation.
[b] From Ref. [39].
[c] From Ref. [40].
[d] From Ref. [41].
[e] Reference for Ir–Ir.
[f] Reference for Ir–P.
[g] Reference for Ir–C.
[h] Reference for Ir–O.

tively. Even atomic number of tungsten was smaller than that of iridium by three, $W(CO)_6$ can be a good reference compound because of narrow distribution of W–O distances. The effect of multiple scattering can be included by using backscattering amplitude and phase shift function derived from $W(CO)_6$. Table 1 summarized the range of Fourier filtering to derive the experimental phase shift and backscattering amplitude.

3. Result and discussion

3.1. Ir and EXAFS characterization of tetra-iridium carbonyl clusters attached on THP/SiO_2

Fig. 1 shows IR spectra of carbonyl species on Ir_4/THP/SiO_2 evacuated at various temperatures. ν(CO) of terminal CO were observed at 2096, 2079, 2060, 2029, and 1990 (shoulder) cm^{-1} and that of bridge CO were observed at 1836 and 1811 cm^{-1}, respectively on the IR spectra of Ir_4/THP/SiO_2 evacuated at 298–348 K. When the sample was evacuated at 373 K, IR bands at 2096, 1836, and 1811 cm^{-1} were relatively suppressed and the shoulder band at 1990 cm^{-1} was slightly developed as shown in Fig. 1b–d.

The IR data associated with the bridge CO in Ir_4/THP/SiO_2 clearly suggested that the attached tetra-iridium cluster was coordinated by phosphine ligands because $Ir_4(CO)_{12}$ only has terminal CO and tetra-iridium clusters coordinated by phosphine ligands have bridge CO. IR bands of carbonyl ligands of $Ir_4(CO)_{10}(PPh_3)_2$ were observed at 2064, 2036, 1992 cm^{-1} ($\nu(CO_{terminal})$) and 1827, 1790 cm^{-1} ($\nu(CO_{bridge})$) and those of $Ir_4(CO)_9(PPh_3)_3$ were

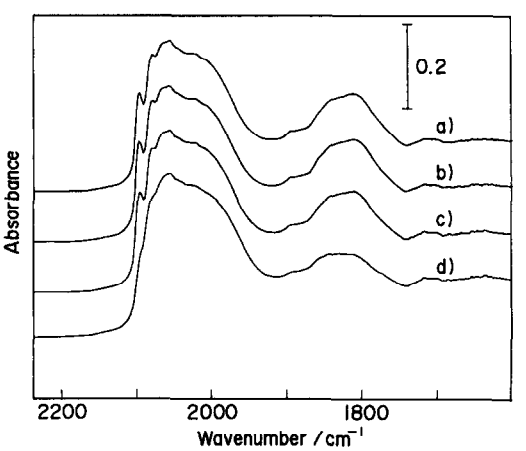

Fig. 1. IR spectra of Ir_4/THP/SiO_2. The sample was evacuated at (a) 298 K, (b) 323 K, (c) 348 K, and (d) 373 K.

observed at 2042, 1998, 1985 cm^{-1} ($\nu(CO_{terminal})$) and 1778, 1777 cm^{-1} ($\nu(CO_{bridge})$), respectively [23]. As the wavenumber of carbonyl ligands of tetra-iridium cluster depend little on the type of phosphine ligands, phenyl phosphine or alkyl phosphine [24], the comparison of IR wavenumber of carbonyl species suggested that tetra-iridium carbonyl clusters on THP/SiO_2 were coordinated by two THP ligands because the wavenumber of IR bands of $Ir_4/THP/SiO_2$ resembled to those of $Ir_4(CO)_{10}(PPh_3)_2$, rather than $Ir_4(CO)_9(PPh_3)_3$.

The comparison of wavenumber between the attached iridium carbonyl clusters and partially substituted iridium carbonyl clusters to THP can provide more clear conclusions. Since it needs sodium metal or potassium hydroxide to synthesize partially substituted iridium carbonyl clusters to phosphine ligands [23], however, it may be difficult to synthesize THP substituted iridium carbonyl clusters by conventional methods because THP was easy to decompose in the presence of sodium metal or potassium hydroxide.

IR bands at 2096 and 2079 cm^{-1} observed on $Ir_4/THP/SiO_2$ can be assigned to mono substituted tetra-iridium carbonyl clusters, $Ir_4(CO)_{11}(THP/SiO_2)$ referred to the IR bands of carbonyl species of $Ir_4(CO)_{11}PPh_3$ at 2096–2086 and 2069–2054 cm^{-1} [25]. The area of the bands at 2096 and 2079 cm^{-1} which were assigned to $Ir_4(CO)_{11}(THP/SiO_2)$ was about 5% of the area of 2060, 2029 and 1990 cm^{-1} bands assigned to $Ir_4(CO)_{10}(THP/SiO_2)_2$. It may be unlike that absorption coefficients of these species were quite different from each other. Hence, IR results suggested that most of $Ir_4(CO)_{12}$ on THP/SiO_2 was coordinated by two THP and about 5% of the $Ir_4(CO)_{12}$ was coordinated by one THP. Tetra-iridium clusters coordinated by one THP may be converted to those substituted by two THP by the evacuation at 373 K because the peaks at 2096 and 2079 cm^{-1} were almost disappeared by the evacuation, accompanied by the increase of 1990 cm^{-1} shoulder band. Hence, the attached tetra-iridium carbonyl clusters on THP/SiO_2 was coordinated by two THP ligands uniformly when the sample was evacuated at 373 K.

IR results also imply that tetra-iridium clusters did not decompose to iridium monomer or dimer species. Because the IR spectrum was not changed by the evacuation except the decreasing of the band at 2096 cm^{-1} and the band of bridge CO. If the clusters were decomposed to iridium dimer or monomer, IR band around 1940 cm^{-1} should be observed [24]. Hence, $Ir_4/THP/SiO_2$ was not a mixture of Ir_4, Ir_2, and Ir_1 complexes and most of attached tetra-iridium clusters remained their cluster frameworks.

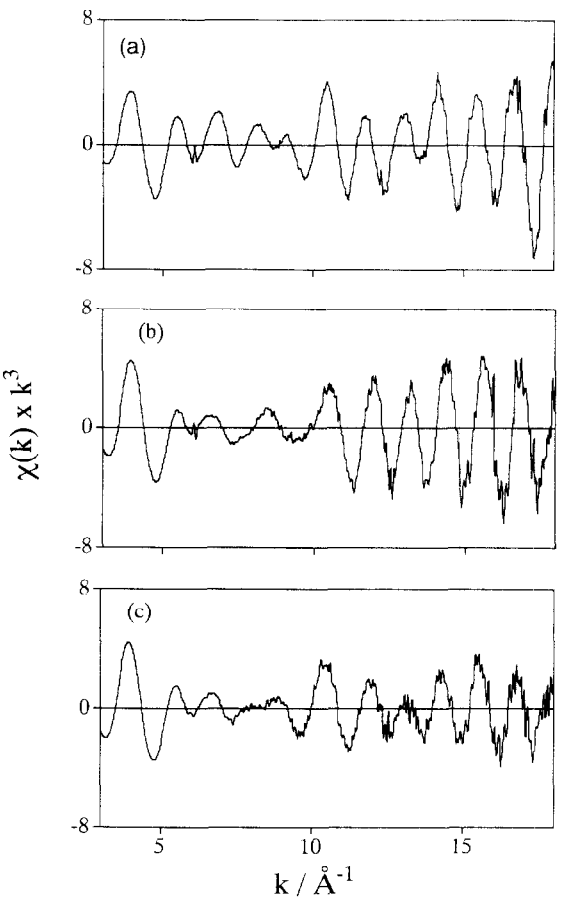

Fig. 2. k^3 weighted Ir L_{III} edge EXAFS function ($\chi(k)\times k^3$) of (a) $Ir_4(CO)_{10}(PPh_3)_2$, (b) $Ir/THP/SiO_2$ evacuated at 298 K, and (c) $Ir_4/THP/SiO_2$ evacuated at 373 K.

XRD analysis showed that there are two kind of bridge CO on the bidentated phosphine substituted tetra-iridium carbonyl clusters [26]. One is a bridge CO between iridium atoms one of which is coordinated by phosphine ligand and the other of which is not coordinated by phosphine ligand (type I). The other is a bridge CO between iridium atoms both of which are coordinated by phosphine ligands (type II). Phosphine ligands donate electrons to iridium atoms to decrease the wavenumber of ν(CO) of coordinated CO, which suggests that wavenumber of ν(CO) of type II is lower than that of type I. Hence IR bands at 1836, and 1811 cm^{-1} can be assigned to type I and type II bridge CO of $Ir_4/THP/SiO_2$, respectively.

As mentioned previously, when the sample was evacuated at 373 K, band intensity of bridge CO at 1836, and 1811 cm^{-1} decreased, which suggested that some bridge CO were removed by the evacuation to form a coordinatively unsaturated tetra-iridium carbonyl clusters. The peak intensity of bridge CO became half or one third of the original intensity by the evacuation. It meant that one or two bridge CO were desorbed by the evacuation. Even both the intensity of bands at 1836 and 1811 cm^{-1} was decreased by the evacuation, the intensity of the band at 1811 cm^{-1} (type II bridge CO) decreased faster than that of the band at 1836 cm^{-1} (type I bridge CO). This suggested that type II bridge CO were eliminated easier than type I bridge CO. The type II bridge CO was eventually disappeared by the evacuation at 373 K.

To make insight in the structure of the attached tetra-iridium clusters, EXAFS evaluation has been conducted. Figs. 2–4 show extracted EXAFS functions, Fourier transformed EXAFS functions, and Fourier filtered EXAFS functions with curve fitting results of $Ir_4(CO)_{10}(PPh_3)_2$, $Ir_4/THP/SiO_2$ before and after the evacuation at 373 K, respectively. EXAFS oscillations were observed in high signal/noise ratio up to 18 $Å^{-1}$ in each spectrum as shown in Fig. 2. k range of 3.5–15 $Å^{-1}$ of the EXAFS functions were Fourier transformed as shown in Fig. 3 and R range of 1.2–3.2 Å of Fourier transformed functions were filtered and inverse transformed as shown in Fig. 4 (represented by solid line). Correction of phase shift was not carried out in Fig. 3. In the figures of Fourier transformed EXAFS functions, three peaks were observed at 1.5, 2.0 and 2.3–2.5 Å, respectively. The former two peaks can be assigned to

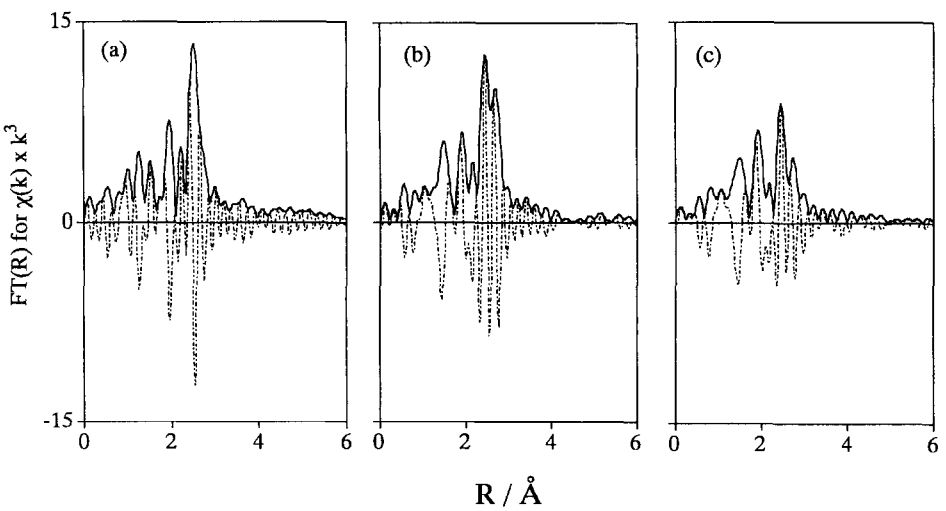

Fig. 3. Fourier transformed k^3 weighted Ir L_{III} edge EXAFS function ($\chi(k) \times k^3$) of (a) $Ir_4(CO)_{10}(PPh_3)_2$, (b) $Ir/THP/SiO_2$ evacuated at 298 K, and (c) $Ir_4/THP/SiO_2$ evacuated at 373 K. The R range for Fourier filtering was 1.2–3.2 126 Å in each spectrum.

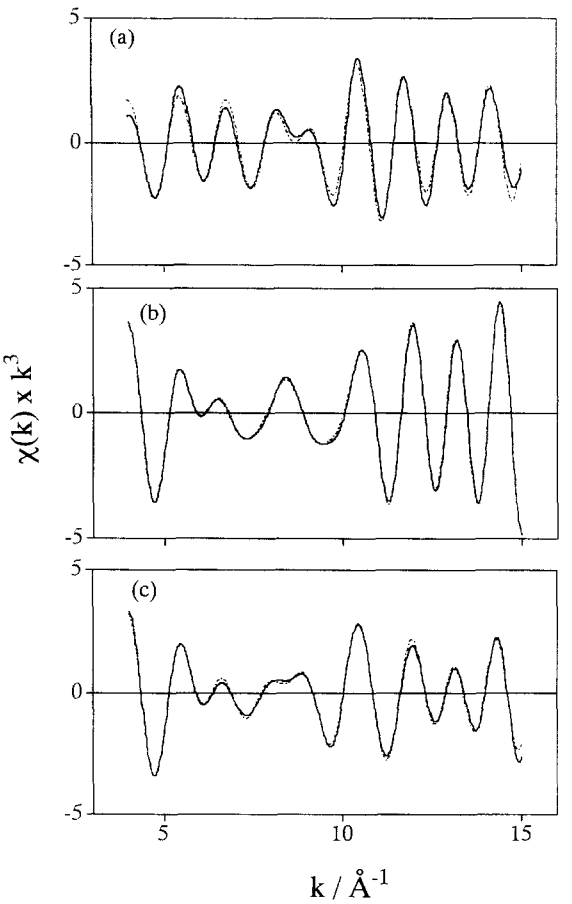

Fig. 4. Fourier filtered k^3 weighted Ir L_{III} edge EXAFS function ($\chi(k)\times k^3$) of (a) $Ir_4(CO)_{10}(PPh_3)_2$, (b) $Ir/THP/SiO_2$ evacuated at 298 K, and (c) $Ir_4/THP/SiO_2$ evacuated at 373 K. R-range for Fourier filtering was 1.2–3.2 Å in each spectrum.

Ir–C, Ir–P contribution and the peak at 2.3–2.5 Å can be assigned to the overlap of the contributions of Ir–Ir and Ir–O (of CO). The peak height of Ir–P and Ir–C contribution were almost the same in each spectrum. On the contrary, the peak height of the Ir–Ir and Ir–O contributions of $Ir_4/THP/SiO_2$ after the evacuation at 373 K was about 60% of that of $Ir_4(CO)_{10}(PPh_3)_2$ and $Ir_4/THP/SiO_2$ before the evacuation.

The filtered EXAFS functions were fitted by four shells, Ir–Ir, Ir–P, Ir–C and Ir–O. The fitting parameters were inter atomic distance (R), coordination number (CN), collection of threshold energy (ΔE_0) and Debye–Waller like factor ($\Delta\sigma$). The best fit was represented by the doted line in Fig. 4. Calculated functions reproduced the observed EXAFS functions well.

Table 2 summarized structural parameters and residual factors derived from EXAFS analysis of $Ir_4(CO)_{12}$, $Ir_4(CO)_{10}(PPh_3)_2$, $Ir_4/THP/SiO_2$ before and after the evacuation at 373 K, after ethene hydroformylation reaction and after propene oxidation reaction. Coordination number of Ir–Ir and Ir–P of fresh $Ir_4/THP/SiO_2$ were calculated to be 2.9 and 0.5, respectively, which suggest that tetra-iridium carbonyl clusters remained their framework and were coordinated by two THP grafted on the silica surface. Ir–Ir distance of $Ir_4/THP/SiO_2$ was calculated to be 2.72 Å, which was longer than that of $Ir_4(CO)_{12}$ by 0.05 Å [27] and similar to that of $Ir_4(CO)_{10}(PPh_3)_2$ [26].

In the case of tetrarhodium carbonyl clusters, Rh–Rh distance of $Rh_4(CO)_8(P(OPh)_3)_4$ is shorter than that of $Rh_4(CO)_{12}$ because of the coordination of phosphine ligands [27]. On the contrary Rh–Rh distance was slightly elongated by the attachment on THP/SiO_2 [16–18], where the attached tetrarhodium clusters on THP/SiO_2 were coordinated by two THP to distort the cluster framework. By contrast to the attached tetrarhodium carbonyl clusters, Ir–Ir distance of the attached tetra-iridium clusters were almost the same as that of $Ir_4(CO)_{10}(PPh_3)_2$. Ir–Ir distance was elongated by the coordination of phosphine ligands both in crystal [27] and on THP/SiO_2. Hence, in the case of tetra-iridium carbonyl clusters, elongation of Ir–Ir distance by the coordination of phosphine ligands is a general phenomenon and additional elongation of Ir–Ir distance was not observed by the attachment on THP/SiO_2.

As shown in Fig. 3(c), peak intensity at 2.5 Å of the evacuated sample at 373 K was decreased to about 60% of that of fresh $Ir_4/THP/SiO_2$. There are two possibilities to explain this result. One possibility is that the CN of Ir–Ir contribution was decreased by the evacuation, which suggest that the attached tetra-iridium clusters were decomposed by the evacuation at 373 K.

The other possibility is that the CN of Ir–Ir contribution was not decreased but the Debye–Waller factor of this contribution was increased implying that the tetra-iridium cluster framework should be remained after the evacuation. The curve fitting analysis supported the latter possibility. The CN and the Fs of Ir–Ir contribution changed from 2.9 to 2.5 and 0.000 to 0.045 Å, respectively. As the error of CN is estimated to ± 0.4, CN of Ir–Ir of $Ir_4/THP/SiO_2$ was almost unchanged and the $\Delta\sigma$ was efficiently increased by the evacuation. When the $\Delta\sigma$ was fixed at smaller value such as 0.000 Å, the calculated EXAFS function did not reproduce the observed EXAFS function. Hence we concluded that tetra-iridium frameworks were re-

Table 2
Structural parameters of Ir carbonyl clusters

Compound/shell	C.N.	R/Å	ΔE_0/eV	$\Delta\sigma$/Å	*R* factor (%)
$Ir_4(CO)_{12}$ [a]					
Ir–Ir	3.0	2.68	−5.0	0.0	
Ir–C	3.0	1.90	−5.4	0.0	6.5
Ir–O	3.0	3.05	1.5	0.0	
$Ir_4(CO)_{10}(PPh_3)_2$ [b]					
Ir–Ir	2.7	2.73	−9.1	0.030	
Ir–P	0.50	2.37	−5.2	0.040	7.3
Ir–C	2.9	1.90	−10.7	0.080	
Ir–O	1.5	3.09	5.8	0.073	
$Ir_4/THP/SiO_2$ (fresh)					
Ir–Ir	2.9	2.72	4.2	0.000	
Ir–P	0.50	2.38	−1.5	0.044	
Ir–C	2.8	1.91	−10.4	0.072	3.5
Ir–O	2.4	3.03	−2.8	0.000	
$Ir_4/THP/SiO_2$ (evac. at 373 K)					
Ir–Ir	2.5	2.73	−0.9	0.045	
Ir–P	0.46	2.37	−1.9	0.040	2.5
Ir–C	2.1	1.90	−13.3	0.031	
Ir-O	2.1	3.06	0.0	0.020	
$Ir_4/THP/SiO_2$ (after hydroformylation reaction) [c]					
Ir–Ir	2.3	2.74	3.1	0.046	
Ir–P	0.50	2.38	−1.2	0.040	7.3
Ir–C	2.8	1.91	−11.6	0.059	
Ir–O	2.2	3.05	−0.8	0.0	
$Ir_4/THP/SiO_2$ (after oxidation reaction) [d]					
Ir–Ir	2.3	2.73	2.1	0.043	
Ir–P	0.50	2.35	−6.3	0.040	
Ir–C	2.3	1.90	−12.0	0.030	10.8
Ir–O	1.9	3.05	0.57	0.0	

[a] Average distances of Ir–Ir, Ir–C and Ir–O, obtained by XRD analysis, are 2.693, 1.87 and 3.01 Å, respectively [21].
[b] Average distances of Ir–Ir, Ir–P, Ir–C of terminal CO, and Ir–C of bridge CO obtained by XRD analysis are 2.73, 2.36, 1.85 and 2.10 Å respectively [22].
[c] Reaction conditions; $T = 353$ K, $p(H_2) = p(CO) = p(C_2H_4) = 13.3$ kPa, reaction period = 24 h.
[c] Reaction conditions; $T = 353$ K, $p(O_2) = p(C_3H_6) = 13.3$ kPa, reaction period = 24 h.

mained and structurally distorted by the partial decarbonylation due to the evacuation at 373 K.

The CN of Ir–C decreased by the evacuation at 373 K, from 2.8 to 2.1, while the CN of Ir–O little decreased from 2.4 to 2.1. Ir–C contribution came from both terminal and bridge CO and Ir–O contribution mainly came from terminal CO because of the lens effect of carbon between iridium and oxygen [21]. Hence, this result suggested that bridge CO was desorbed by the evacuation at 373 K while the terminal CO were little desorbed, which was consistent with the IR result showing that one or two bridge CO were removed during the evacuation at 373 K.

The structural parameters of $Ir_4/THP/SiO_2$ before and after hydroformylation of ethene and oxidation of propene were almost unchanged. These results implied that tetra-iridium framework of $Ir_4/THP/SiO_2$ remained basically unchanged and was not degraded under the condition of catalytic reactions of hydroformylation reaction (323–353 K, $p(H_2) = p(CO) = p(C_2H_4) = 13.3$ kPa) and oxidation reaction (323–353 K, $p(O_2) = p(C_3H_6) = 13.3$ kPa).

A proposed structure of $Ir_4/THP/SiO_2$ before and after the evacuation at 373 K are depicted in Scheme 1. Almost all of tetra-iridium carbonyl clusters were coordinated by two THP to be anchored on the surface with remaining cluster framework. When $Ir_4/THP/SiO_2$ was evacuated at 373 K, one or two bridge CO were desorbed and tetra-iridium cluster framework was distorted without decomposition to other species such as Ir monomer, dimer or metal particle. The structure of attached tetra-iridium clusters remain unchanged under the reaction conditions of hydroformylation and oxidation reaction.

3.2. Catalytic activities of $Ir_4/THP/SiO_2$

As shown in Fig. 5, propanal and ethane were produced catalytically during the ethene hydroformylation reaction on $Ir_4/THP/SiO_2$ before and after the evacuation at 373 K under the reaction atmosphere of $p(H_2) = p(CO) = p(C_2H_4) = 13.3$ kPa. The evacuation of $Ir_4/THP/SiO_2$ at 373 K substantially affected catalytic performances such as reaction rate and selectivity of the propanal formation. The rate of propanal formation on the catalyst evacuated

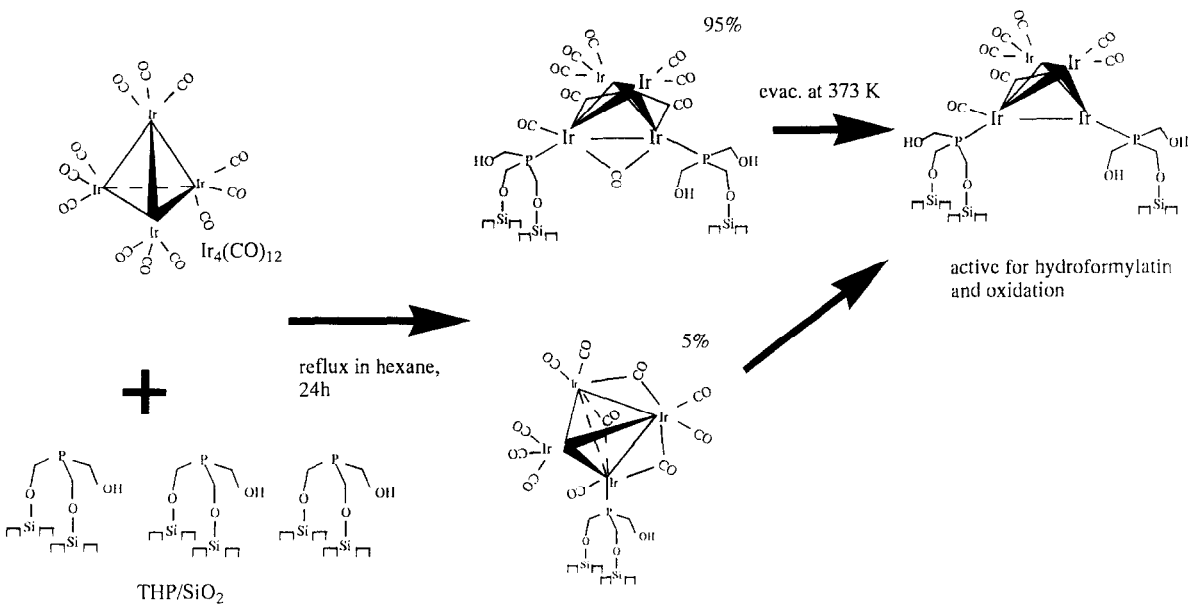

Scheme 1. Proposed structures of $Ir_4(CO)_{12}$ attached on THP/SiO_2.

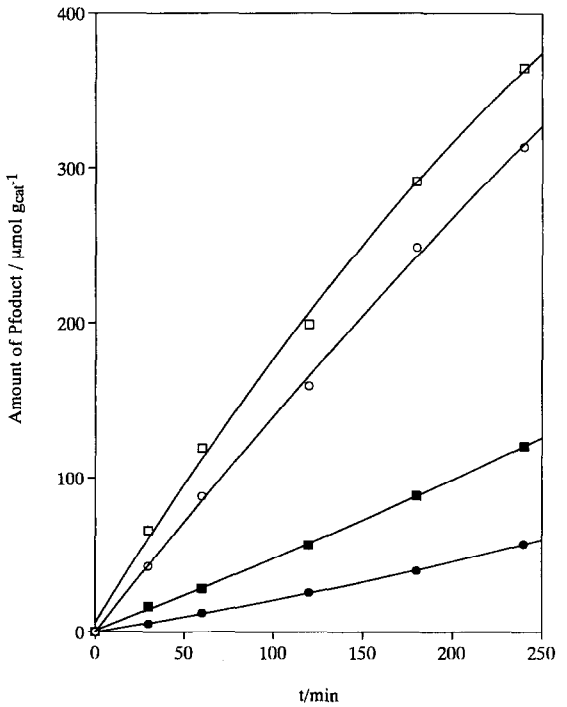

Fig. 5. Amount of products of hydroformylation reaction on $Ir_4/THP/SiO_2$ as a function of reaction period; (○) propanal formation and (□) ethane formation on $Ir_4/THP/SiO_2$ evacuated at 373 K, (●) propanal formation and (■) ethane formation on $Ir_4/THP/SiO_2$ evacuated at 298 K.

at 373 K was six times as fast as that on the fresh catalyst. The rate of propanal formation on the evacuated and unevacuated catalyst was 1.5 mmol g_{cat}^{-1} min^{-1} (TOF = 1.6×10^{-4} s^{-1}) and 0.24 mmol g_{cat}^{-1} min^{-1} (TOF = 2.6×10^{-5} s^{-1}), respectively. The selectivity of propanal formation was improved to 50% from 30% by the evacuation at 373 K.

The rate and selectivity of propanal formation on both evacuated and unevacuated catalyst were slightly changed during catalytic reaction. In the case of unevacuated $Ir_4/THP/SiO_2$, reaction rate of propanal and ethane formation were increased as increase reaction period and selectivity for propanal formation was slightly increased. The increase of the reaction rate and selectivity on unevacuated $Ir_4/THP/SiO_2$ may be caused by the structural transformation due to partial decarbonylation of $Ir_4/THP/SiO_2$ catalyst during hydroformylation reaction. As the reaction was carried out at 353 K, the tetra-iridium clusters on THP/SiO_2 may be changed gradually to the distorted tetra-iridium clusters similar to those evacuated at 373 K. In the case of the evacuated catalyst, rate of propanal formation was almost unchanged during the reaction and that of ethane was decreased as increased the reaction period. The rate of ethane formation was 2.2 mmol g_{cat}^{-1} min^{-1} (TOF = 2.3×10^{-4} s^{-1}) at the initial stage and the rate was gradually decreased to be 1.5 mmol g_{cat}^{-1} min^{-1} (TOF = 1.6×10^{-4} s^{-1}) after 100 min. The decrease of the rate of ethane formation caused the increase of the selectivity of propanal and the selectivity of the propanal was 50% at steady state (after 100 min).

Fig. 6 shows IR spectra of coordinated CO on the evacuated $Ir_4/THP/SiO_2$ under hydroformylation reaction condition. Besides the IR bands observed under vacuum, a new band appeared at 2140 cm^{-1}. The band intensity gradually increased as the exposure period increased. This band disappeared reversibly by the evacuation of reactant gases. The decrease of the reaction rate of ethane formation may relate to the

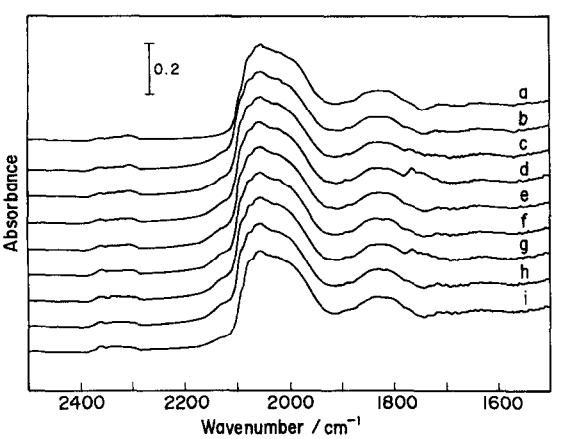

Fig. 6. IR spectra of $Ir_4/THP/SiO_2$ under hydroformylation reaction condition. (a) The sample was evacuated at 373 K for 60 min. After (a) the sample was exposed to reactant gas of ethene hydroformylation ($p(H_2) = p(CO) = p(C_2H_4) = 13.3$ kPa) for (b) 30 min, (c) 60 min, (d) 120 min, (e) 180 min, (f) 240 min, (g) 300 min, and (h) 360 min, (i) after (h), the sample was evacuated at 353 K for 30 min. Each spectrum was measured at 353 K.

increase of band intensity at 2140 cm^{-1} by the comparison of Figs. 5 and 6. On the other hand intensity of bridge CO at 1836 and 1811 cm^{-1} which was decreased by the evacuation at 373 K did not increase during the reaction. The distortion of tetra-iridium framework may weaken the strength of CO adsorption to increase the reaction rate and selectivity for propanal formation. It is expected that active site for hydroformylation was not blocked by CO because CO was adsorbed weakly and that active site for hydrogenation was blocked by weakly adsorbed CO whose IR band was located at 2140 cm^{-1}. It is said that reaction site of hydrogenation is larger than that of hydroformylation and when the catalyst surface or active site was partially blocked the selectivity of aldehyde formation was increased [2]. In this case, weakly adsorbed CO partially blocked the tetra-iridium active site to increase the selectivity toward propanal. Such phenomena was also observed on the case of attached $Rh_4(CO)_{12}$ on THP/SiO_2 [16–18]. In the reaction conditions of hydroformylation, CO weakly adsorbed on tetra-rhodium active site to prevent hydrogenation reaction.

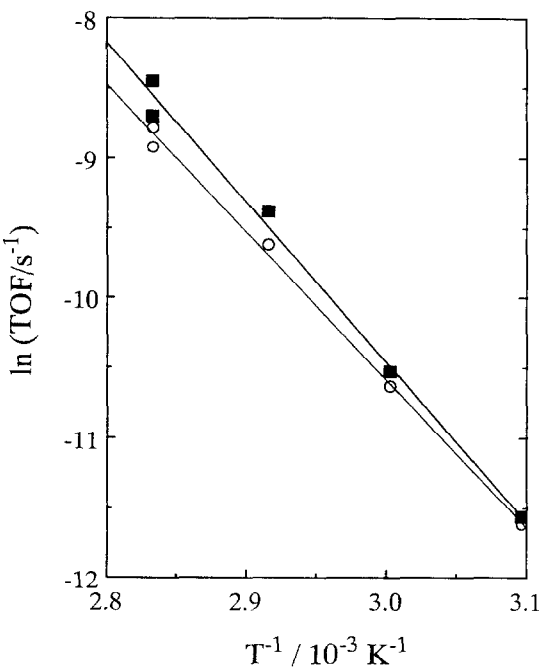

Fig. 7. Arrhenius plots for ethene hydroformylation on $Ir_4/THP/SiO_2$ evacuated at 373 K. (□) Turn over frequency (TOF) of propanal formation, (○) TOF of ethane formation (side reaction of ethene hydroformylation). TOF was calculated by dividing the formation rate by total amount of iridium atoms.

Fig. 7 shows Arrhenius plots for hydroformylation of ethene on $Ir_4/THP/SiO_2$ evacuated at 373 K. The activation energy of propanal and ethane formation was calculated to be 91 and 76 kJ mol^{-1}, respectively. The rate of propanal and ethane formation was almost the same in a temperature range of 323–353 K. The selectivity for propanal formation was slightly decreased as decrease the reaction temperatures. In the case of hydroformylation reaction on iridium catalysts, the activation energy of propanal formation and ethane formation was reported to be similar to each other and the activation energies were similar to those reported previously [28–32].

Hydroformylation reaction on homogeneous iridium complexes derived from $IrCl_3$ [29,30] and supported iridium metal catalyst [31] and iridium sulfide catalyst [32] were investigated. Both homogeneous and heterogeneous catalysts, the catalytic reaction proceeded above 373 K and the selectivity of the aldehyde was less than 20% and the activation energy for aldehyde formation was larger than that of alkane formation which cause the decrease of selectivity as increase the reaction temperature. On the other hand, hydroformylation reaction proceed below 373 K on $Ir_4/THP/SiO_2$ catalyst reported here and the selectivity for propanal formation was 50% which was about 2.5 time larger than other Ir catalyst and which was not decrease very much as increase reaction temperatures. Hence, $Ir_4/THP/SiO_2$ reported here may be one of the most active and selective Ir catalyst for hydroformylation.

$Ir_4/THP/SiO_2$ evacuated at 373 K exhibit catalytic activity for partial oxidation of propene. The catalytic activity appeared by the evacuation at 373 K and $Ir_4/THP/SiO_2$ without evacuation was not active for oxidation of propene. Fig. 8 shows Arrhenius plots for oxidation of

propene. The activation energy for acetone and CO_2 formation was 52 and 108 kJ mol^{-1}, respectively. At 353 K, TOF of acetone and CO_2 formation were 6.7×10^{-6} s^{-1} and 1.77×10^{-5} s^{-1}, respectively. Considering that three mole of CO_2 are formed from one mole of propene ($C_3H_6 + \frac{9}{2}O_2 \rightarrow 3CO_2 + 3H_2O$), selectivity of acetone formation at 353 K was calculated to be 53%. Formation of CO_2 was not observed at 323 K and the selectivity of acetone formation was 100% at that temperature. Induction period of acetone formation was not observed and acetone was produced linearly without deactivation.

As mentioned previously, the catalytic activity was appeared by the evacuation at 373 K similar to the case of hydroformylation. Distortion of the tetra-iridium framework may originate the catalytic activity of oxidation reaction. Activation process by the distortion of the cluster framework may be a general phenomena in many kinds of catalytic reactions.

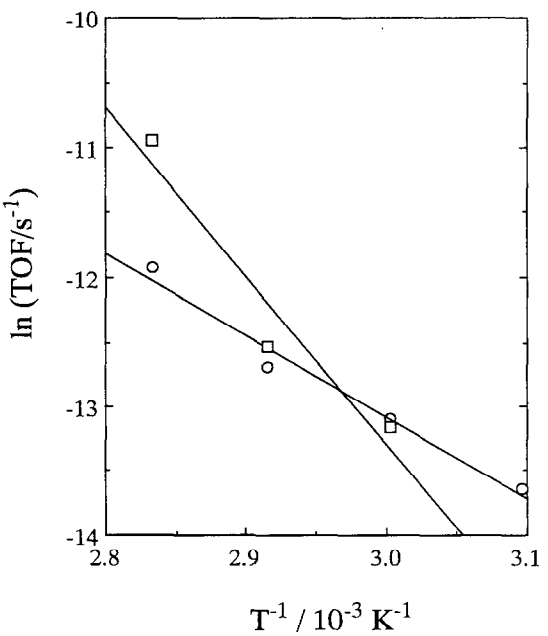

Fig. 8. Arrhenius plots for propene oxidation on Ir_4/THP/SiO_2 evacuated at 373 K. (○) Turn over frequency (TOF) of acetone formation, (□) TOF of CO_2 formation (side reaction of ethene hydroformylation). TOF was calculated by dividing the formation rate by total amount of iridium atoms.

Iridium dioxygen complexes are know as Vaska complex and their structure and reactivity has been investigated [33]. Stoichiometric oxygen insertion reaction between coordinated oxygen and olefin ligand occurs [34] and catalytic oxidation of styrene [35], cyclohexene [36], and tetramethylethylene [37] proceed on these complexes. Recently, Ir dimmer complex with bridge coordinating dioxide (Ir–O–O–Ir) was synthesized [38]. In the case of Ir_4/THP/SiO_2, such kind of coordinating dioxygen may exist during the catalytic oxidation reaction.

The cluster structure remained during the catalytic reaction. The structural parameter derived by Ir L_{III} edge EXAFS after hydroformylation and oxidation reaction did not changed as discussed previously. Distance and coordination number of Ir–Ir and Ir–P shells were not changed. Further, IR spectra during hydroformylation reaction also suggest that the Ir cluster structure remained during hydroformylation reaction as shown in Fig. 6. Except the appearance of IR bands of weakly adsorbed CO at 2140 cm^{-1} under the reaction condition, IR bands of coordinated carbonyl species at 2096–1990 cm^{-1} (terminal) and at 1836 and 1811 cm^{-1} (bridge) remain unchanged.

Kinetic study on well characterized attached tetra-iridium carbonyl clusters revealed that the catalytic hydroformylation and oxidation proceed on the distorted clusters. The cluster framework remained during reaction conditions and the distortion of the cluster framework originated the catalytic activity. Comparison with other conventional iridium catalysts showed that Ir_4/THP/SiO_2 was one of the most active and selective catalyst. This report provides an example of active iridium clusters attached on oxide surface.

4. Conclusion

(1) $Ir_4(CO)_{12}$ attached on THP/SiO_2 remain their cluster frameworks and coordinated by two THP ligands grafted on silica surface. When the

$Ir_4/THP/SiO_2$ was evacuated at 373 K, the tetra-iridium framework was structurally distorted accompanied with substantial increase Debye–Waller factor of Ir–Ir contribution.

(2) The distortion of the tetra-iridium framework was resulted in the removal of one or two bridge CO and the strength of CO adsorption was weakened due to the distortion of the cluster framework.

(3) The distorted clusters on THP/SiO_2 was catalytically active for the olefin hydroformylation and selective oxidation reaction, whereas the original clusters exhibited low catalytic activity.

(4) EXAFS and FTIR characterization and kinetic studies revealed that the catalytic activity of $Ir_4/THP/SiO_2$ was generated by the distortion of the tetra-iridium clusters. $Ir_4/THP/SiO_2$ was more active and selective catalyst than other Ir catalysts reported previously.

References

[1] M. Ichikawa, in: Y. Iwasawa (Ed.), Tailored Metal Catalysis (Reidel, Dordrecht, 1984) p. 138; Polyhedron 7 (1988) 2351.
[2] M. Ichikawa, Adv. Catal. 38 (1992) 283.
[3] Y. Iwasawa, Adv. Catal. 35 (1987) 187.
[4] B.C. Gates, L. Guczi and H. Knozinger (Eds.), Metal Clusters in Catalysis (Elsevier, Amsterdam, 1986).
[5] B.C. Gates, in: M. Moskovits (Ed.), Metal Clusters (Wiley, New York, 1986) p. 283.
[6] Y. Iwasawa, in: Y. Iwasawa (Ed.), Tailored Metal Catalysis (Reidel, Dordrecht, 1984) p. 1.
[7] R. Psaro, C. Dossi, A. Fusi, R. D. Pergola, L. Garlaschelli, D. Roberto, L. Sordelli and R. Ugo, J. Chem. Soc. Faraday Trans. 88 (1992) 369.
[8] S. Kawi, J.-R. Chang and B.C. Gates, J. Phys. Chem. 97 (1993) 5375.
[9] S.D. Maloney, M.J. Kelley, D.C. Koningsberger and B.C. Gates, J. Phys. Chem. 95 (1991) 9406.
[10] F.B.M. van Zon, S.D. Maloney, B.C. Gates and D.C. Kningsberger, J. Am. Chem. Soc. 115 (1993) 10317.
[11] S. Kawi, J.-R. Chang and B.C. Gates, J. Phys. Chem. 98 (1994) 12978.
[12] F.-S. Xiao, Z. Xu, O. Alexeev and B.C. Gates, J. Phys. Chem. 99 (1995) 1548.
[13] S. Kawi, J.-R. Chang and B.C. Gates, J. Am. Chem. Soc. 115 (1993) 4830.
[14] S. Kawi, J.-R. Chang and B.C. Gates, J. Phys. Chem. 97 (1993) 10599.
[15] S. Kawi, J.-R. Chang and B.C. Gates, J. Catal. 142 (1993) 585.
[16] T. Shido, T. Okazaki, M.A. Ulla, T. Fujimoto and M. Ichikawa, Catal. Lett. 20 (1993) 37.
[17] T. Shido, T. Okazaki and M. Ichikawa, Catal. Lett. 17 (1993) 97.
[18] T. Shido, T. Okazaki and M. Ichikawa, J. Catal. 157 (1995) 436.
[19] S. Martinengo, P. Chini and G. Giordano, J. Organomet. Chem. 27 (1971) 389.
[20] P.E. Cattermole, K.G. Orrell and A.G. Osborne, J. Chem. Soc. Dalton. Trans. (1974) 328.
[21] B.K. Teo, EXAFS: Basic Principles and Data Analysis (Springer-Verlag, Berlin, 1986).
[22] D.C. Koningsberger and R. Prins (Eds.), X-ray Adsorption (Wiley-Interscience, New York, 1988).
[23] M. Angoletta, L. Malatesta and G. Gaglio, J. Organomet. Chem. 94 (1975) 99.
[24] P.E. Cattermole, K.G. Orrell and A.G. Osborne, J. Chem. Soc., Dalton Trans. (1974) 328.
[25] G.F. Stuntz and J.R. Shapley, Inorg. Chem. 15 (1976) 1994.
[26] V. Albano, P. Bellon and V. Scatturin, J. Chem. Soc. Chem. Commun. (1967) 730.
[27] M.R. Churchill and J.P. Hutchinson, Inorg. Chem. 17 (1978) 3528.
[28] G. Ciani, L. Garlaschelli, M. Manassero and U. Sartorelli, J. Organomet. Chem. 129 (1977) C25.
[29] M. Yamaguchi, SHOKUBAI (Catalyst) 11 (1969) 180; 9 (1967) 160.
[30] M. Alvila, T.A. Pakkane and T.T. Pakkanen, J. Mol. Catal. 73 (1992) 325.
[31] K. Takeuchi, T. Hanaoka, T. Matsuzaki, M. Reinikainen and Y. Sugi, Catal. Lett. 8 (1991) 253.
[32] S.S.C. Chaunag, Appl. Catal. 66 (1990) L1.
[33] L.Vaska, Accounts Chem. Res. 1 (1968) 335.
[34] V.W. Day, W.G. Klemperer, S.P. Lockledge and D.J. Main, J. Am. Chem. Soc. 112 (1990) 2031.
[35] K. Takao, Y. Fujiwara, T. Imanaka and S. Teranishi, Bull. Chem. Soc. Jpn. 43 (1970) 1153.
[36] W. Strohmeier and E. Eder, J. Organomet. Chem. 94 (1975) C14.
[37] J.E. Lyons and J.O. Turner, J. Org. Chem. 18 (1972) 2881.
[38] J. Xiao, B.D. Santarsiero, B.A. Vaartstra and M. Cowie, J. Am. Chem. Soc. 115 (1993) 3212.
[39] J. Donohue, The Structure of the Elements (Willey, New York, 1974) p. 218.
[40] P. Bird, J.F. Harrod and K.A. Than, J. Am. Chem. Soc. 96 (1974) 1222.
[41] S.W. Kirtley, in: G. Wilkinson (Ed.), Comprehensive Organometallic Chemistry, Vol. 3 (Pergamon, Oxford, 1982) p. 1257.